International Journal of Technology (2018) 4: 695-706
ISSN 2086-9614

SYNTHESIS AND MONTE CARLO SIMULATION OF IMPROVED CONCRETE COMPOSITES FOR ENHANCED X-RAY/GAMMA RAY RADIATION SHIELDING

Ferhat Aziz[1*], Mardiyanto Panitra[1], Abu Khalid Rivai[1]

[1]*Center for Science and Technology of Advanced Materials, BATAN, Kawasan Puspiptek, Serpong, Tangerang, Banten 15314, Indonesia*

(Received: February 2018 / Revised: April 2018 / Accepted: May 2018)

ABSTRACT

Synthesis and Monte Carlo simulation of improved concrete composites as x-ray/gamma ray shielding materials were performed. Samples of shieldings were synthesized using the base materials of Portland-type cement concrete with fillers of alloy steel, Co, Mn, and Cr, mixed separately as additives. The samples were characterized using Scanning Electron Microscopy-Energy Dispersive X-ray Spectrometry (SEM-EDS) to determine the constituent elements quantitatively. Linear attenuation coefficients of the samples were measured in the experiments and also simulated using Monte Carlo transport code MCNP5 in order to evaluate their shielding performance. The results of the experimentation and computer simulation reveal concrete with alloy steel added as having the best shielding properties, although concrete with other fillers added also exhibited enhanced shielding performance. It was demonstrated that 6.06 w% of fillers enhanced the x-ray/gamma ray shielding capability of ordinary concrete composites by improving their attenuation coefficient values by 40–60%.

Keywords: Attenuation coefficient; Concrete composites; Monte Carlo simulation; Radiation shielding; Synthesis

1. INTRODUCTION

Radiation is a form of energy that moves from its source to its surroundings. It derives from unstable atoms or can be produced by machines. Radiation travels from its source in the form of energy waves or energized particles. Based on the ability of ionization, radiation is divided into two types, i.e. ionizing and non-ionizing radiation. Ionizing radiation is radiation that can cause the ionization process (the formation of positive ions and negative ions) when interacting with a material. Included in ionizing radiation are alpha, beta, and neutron particles, and gamma and x-rays. There are many kinds of non-ionizing radiation, namely radio waves, microwaves, infrared, visible light, and ultraviolet (Knoll, 2000; Arpansa, 2014).

Nuclear radiation is ionizing radiation. It can be generated from many sources, both natural and man-made, such as accelerators, radioisotopes, and reactors. Ionizing radiation has the potential to be both harmful and useful. The emergence of ionizing radiation from its source and interaction with human tissue or instruments can have a negative impact since it can cause disease or damage. By contrast, such radiation can also be useful when used in fields such as nuclear medicine, medical diagnosis, industrial tracing, nondestructive testing, and radiography. Due to its potential adverse effects, nuclear radiation should be properly managed and shielded from those involved in working with it (Kim & Jung, 2013). Adequate protection is thus the

*Corresponding author's email: ferhat@batan.go.id, Tel. +62-21-7560922, Fax. +62-21-7560926
Permalink/DOI: https://doi.org/10.14716/ijtech.v9i4.1723

first priority when handling radiation sources (IAEA, 2014).

X-rays/gamma rays generated by a source of radiation from either a nuclear reactor or other sources should be shielded to prevent harm to the environment. Gamma rays, x-rays, visible light, and radio waves are all types of electromagnetic radiation. Electromagnetic radiation can be viewed in terms of a stream of photons, which are massless particles, each traveling in a wave-like pattern and moving at the speed of light. The main difference is their source: x-rays are emitted by electrons outside the nucleus of an atom, while gamma rays are emitted by the excited nucleus (Knoll, 2000). The other difference lies in their energies and wavelengths. Gamma-ray photons have the highest energy in the spectrum of electromagnetic radiation and their waves have the shortest wavelength. There is however some overlap with x-rays with regard to their energy and frequency range (Lumen Learning, 2018). For example, the energy range employed in the supervoltage and megavoltage x-rays used in linacs (Kim et al., 2018) is greater than the energy of many gamma-emitting radioisotopes. Therefore, from a shielding point of view, they are often used within the same category (Kozlovska et al., 2015). Furthermore, since both gamma rays and x-rays are electromagnetic waves of photons that undergo the same mode of interactions in a shielding material, such as the photoelectric effect, Compton scattering, and pair production (Nikjoo et al., 2012), they are treated in the same manner in a Monte Carlo simulation and experimentation.

The principle of radiation shielding is to reduce the intensity of external radiation to an acceptable level. A good x-ray/gamma ray shielding material should have a high value of photon attenuation coefficients and the irradiation effects on its mechanical properties should be small. Many types of photon shielding have been produced, using different material compositions. These have ranged from classic ones such as concrete to more advanced materials such as custom-made shielding constructed from heavy metals dispersed inside organic polymers (Erol et al., 2016; Aminian et al., 2017; El-Kameesy et al., 2017; Jubier, 2017). Shielding has also been produced using alkali minerals (Kumar et al., 2012), the radiation-shielding properties of which have been compared with those of concretes.

Concrete composite is both excellent and inexpensive and is also the shielding material most widely used in nuclear plants, laboratory hot cells, and medical facilities. It is usually used as the main constituent of building construction material (Oto & Gür, 2013). Yet although concrete is very widely used, this does not mean it has no deficiencies. It has a number of characteristic drawbacks that should be improved, such as the considerable variability in its composition and water content that results in uncertainty in predictions of radiation distribution and attenuation in the shield. It is therefore imperative that such shortcomings be reduced by a proper synthesization process, on account of which the shielding performance of cement-based concrete composite can be enhanced. Continuous research should be carried out to improve the quality of concrete composites with both computer modeling and laboratory experimentation.

In order to enhance the shielding performance of concrete composites, some researchers have used supplementary mineral additives such as barite and witherite (Fugaru et al., 2015). In this study, however, we add different materials as fillers, i.e., the transition metals of Co, Mn, Cr, and alloy steel, to improve the attenuating properties of the concrete composite. The first reason is that these transition metals are abundant and easily found. Second, they have higher densities than alkaline minerals such as barite or witherite, which is a prime requirement for good x-ray/gamma ray shielding (Al-Hamarneh, 2017); as such, they enable some space to be saved. Although lead is a well-known material for use in x-ray/gamma ray shielding, we intentionally exclude it as a potential additive material here since it is toxic and non-environmentally friendly. Lead is opaque to visible light and thus it is difficult to see through the cement-based

concrete shields during manufacturing. Moreover, the size of the lead aggregate will affect the magnitude of the attenuation coefficient and the mechanical strength of the concrete.

In the present work, both computer modeling of the shielding and laboratory experimentation were performed. The computer simulation was carried out using Monte Carlo n-particle transport code MCNP5 (X-5 Monte Carlo Team, 2003) to calculate the linear attenuation coefficients. The results were compared with the linear attenuation of concrete composite samples measured using the conventional film radiography method.

2. EXPERIMENTAL METHODS

This study involved laboratory experimentation to synthesize the improved concrete composites followed by the Monte Carlo method of simulation. The experimentation work was conducted using concrete composites as shielding materials with different fillers at various densities as additives.

A set of experiments were conducted to measure the x-ray intensities before and after passing through the constructed shields. The attenuation coefficient of each shielding material composite could then be calculated. For comparison, computer simulation with a general-purpose particle transport code MCNP5 was performed. If a discrepancy between the experimental result and that of the simulation was considered unacceptable, then the process was repeated, ensuring the correct inputting of the Monte Carlo input and the appropriate mixing and stirring of materials. The whole process was conducted in accordance with the flow diagram as shown in Figure 1.

2.1. Laboratory Experiments

For the laboratory experiment, five concrete composite samples with the addition of four filler variations, i.e., Co, Cr, Mn, alloy steel, and a concrete without filler, were prepared. Concrete was chosen because it has good shielding properties and is inexpensive and readily available. In our experiments, each sample was produced with six varied thicknesses, namely 2, 4, 6, 8, 10, and 12 mm. A thicker sample was not prepared since any changes in linear attenuation coefficient values beyond a thickness of 1.2 cm (12 mm) tend to be less significant due to the asymptotic behavior of attenuation in the materials. The basic materials for the concrete were Portland-type cement, sand, and water. The samples were prepared with mass ratios for cement: sand: water: filler of 1: 1.5: 0.6: 0.2, or by weight percentage of 30.30: 45.46: 18.18: 6.06, respectively. The cement, sand, and filler were weighed and placed in a container and stirred until evenly distributed. Water was then slowly added while continuously stirring. The resultant dough was then inserted into a mold, flattened, and left to dry at room temperature for 24 hours.

The sample materials (cement, sand, Co, Cr, Mn, alloy steel) were characterized using Scanning Electron Microscopy-Energy Dispersive X-ray Spectrometry (SEM-EDS) to determine the constituent elements quantitatively. The characterization data were then used as one of the MCNP5 program inputs.

The volume, mass, and density of the samples with each filler and thickness variation were measured. The value of the density was obtained using the Equation 1, which was also used to derive the inputs for the Monte Carlo simulation.

$$\rho = \frac{m}{v} \tag{1}$$

where ρ is the density (g cm^{-3}); m is the mass (g); and v is the volume (cm^3).

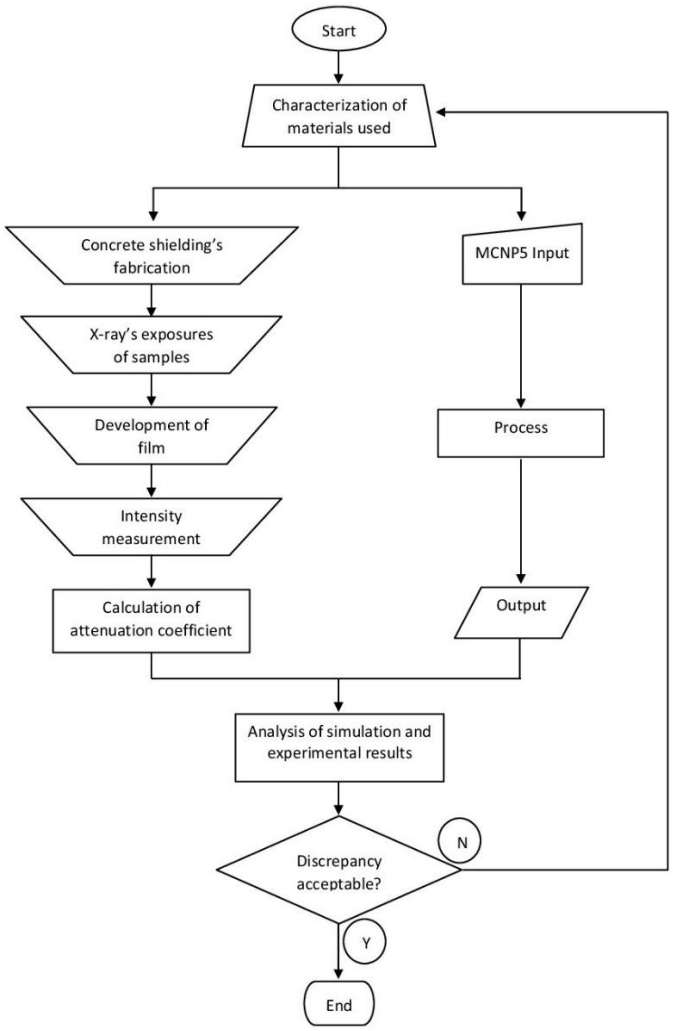

Figure 1 Flow diagram of the synthesis and simulation

The x-ray absorption ability of the samples was tested using an x-ray radiography facility at the Center for Empowerment of Informatics and Nuclear Strategic Area of The National Nuclear Energy Agency of Indonesia, in Serpong. The x-ray absorption test was performed twice, firstly for the thicknesses of 2, 4, and 8 mm, and secondly for the thicknesses of 6, 10, and 12 mm.

Film for capturing the image after exposure to x-ray at a distance of 1 m under the x-ray source had previously been set up using a 35 cm × 35 cm cassette in a dark room. After exposure, the film was developed using a chemical solution.

Figure 2 Equipment and facilities used in the experimentation: a balance (left), prepared samples (middle top), densitometer (middle bottom), and x-ray machine (right)

The procedure comprised the following activities: developing, rinsing, fixing, washing, and drying. The initial and final intensities of the film were then measured. For this purpose, a densitometer and a viewer were used. Figure 2 shows the equipment and facilities used during the experimentation.

The linear attenuation coefficient for each size of sample was calculated using the attenuation equation (Equation 2).

$$\mu_l = -\frac{\ln\left(\frac{I}{I_o}\right)}{t} \tag{2}$$

where μ_l is the linear attenuation coefficient (cm^{-1}); I_o is the initial intensity; I is the final intensity; and t is the thickness (cm).

2.2. Computer Simulation

The Monte Carlo N-particle radiation transport computer code MCNP5 was used to investigate the effects of shield thicknesses on the attenuation of the x-ray/gamma-ray photons. In a radiation-shielding simulation, MCNP5 has shown good agreement with experiments as well as with other computer code, as demonstrated by Elbashir et al. (2018) when they analyzed the attenuation coefficients of amino acids samples. As for benchmark calculation in nuclear criticality application, Kim et al. attempted a comparative study with the latest-evaluated nuclear data libraries. They conducted benchmark calculations for 91 criticality problems with the libraries processed for MCNP code. Their results revealed that the evaluated nuclear data libraries of ENDF/B-VI.8 and JENDL-3.3 showed good agreement with the experiments (Kim et al., 2003).

The simulation was carried out with a simple geometry. The material elements were input based on the characterization results obtained using SEM-EDS. Cells, surfaces, and tallies were made in accordance with the results of the experimental data.

The input geometry used in the simulation was in 3-D Cartesian (x,y,z) described by cell cards and surface cards. The cell cards contained information on the materials used and their densities, while the surface cards provided the coordinates of the system and its environment.

The data cards for MCNP5 comprise the source specification, tally, and materials of the samples. In this simulation we used a disk source placed perpendicular to the y-axis that uniformly and mono-directionally emitted photons in the positive y-direction.

In MCNP5, tallying is a process of scoring parameters of interest to provide the required answers. The *Tally* mnemonic used in our study was F2:P, meaning average surface flux of photons with the unit of #/cm^2. As for the specifications of the materials used, we opted for the form of a mass fraction. The data for the constituent atoms and their respective mass fractions were obtained from the results of basic material characterization using SEM-EDS.

3. RESULTS AND DISCUSSION

The mass attenuation of a shielding material is strongly influenced by its density. The higher its value for density, the better a material's ability to absorb radiation. The measurement results for the density of each sample are presented in Figure 3. The figure shows graphically how 6.06 w% of filler added to concrete composites improved their density significantly. The density values obtained from the experiments for the control concrete (concrete without filler) and those with different metal filler additions of alloy steel, Co, Cr, and Mn were 2.5517, 2.7494, 2.7690, 2.8516, and 2.8563 gr/cm^3, respectively.

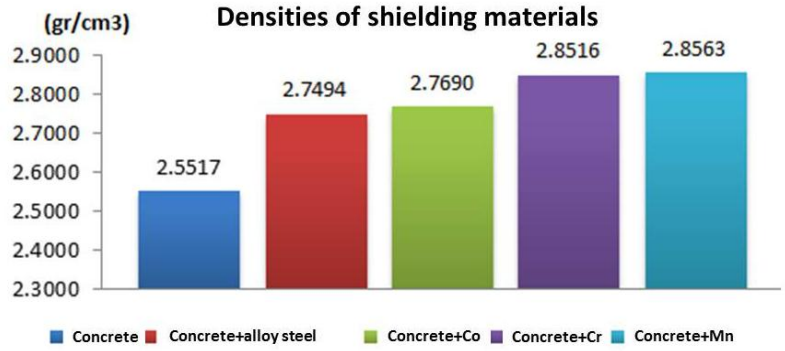

Figure 3 Comparison of the densities of shielding materials

The order of the concrete density values does not correspond to the atomic number sequence or mass of filler; it may be caused by the uneven distribution of the concrete composite in the mold, as indicating the presence of pores. However, the five samples can be categorized as heavy concrete because they have a density value greater than 2.500 gr/cm^3. By definition, a concrete is considered to be a heavy concrete if it has a minimum density value of 2.500 gr/cm^3 (Akkurt et al., 2010; Smolikov et al., 2013; Azeez et al., 2013; Aghamiri et al., 2014).

3.1. Comparison of Initial and Final Intensities

Figure 4 shows that in all cases, as the samples become thicker, the ratios of I/Io (final intensity/initial intensity) become smaller. This also explains that thickness is inversely proportional to I/Io. The thicker the material, the lower the amount of radiation that can penetrate it due to the absorption of photon energy along its thickness. All of the graphs shown in Figure 4 are based on the experimental results obtained using a diagnostic x-ray machine at our Center. The experiments were conducted using an x-ray effective energy of around 42 keV. For ease of comparison, the graph for each sample also contains the control concrete.

The I/Io graph for concrete+Co and concrete without filler shown in Figure 4 (top right) demonstrates a negative exponential curve as a function of thickness. The figure shows a better I/Io curve for concrete+Co, with smaller values than for the control concrete. This explains that concrete containing cobalt absorbs more photons than a common concrete without filler. Figure 4 (bottom left) shows the imperfect negative exponential curve of concrete+Cr. At a thickness of 8 mm, concrete+Cr has a higher I/Io ratio than it should have, and there is a slight bump. This may be due to the fact that the type of chromium used in this experiment was in granular as opposed to powder form, and the densitometer sensor was circular in shape with a larger diameter than the diameter of the granules. As such, an uneven distribution of the elements in the concrete composite may produce less accurate results when measured by the densitometer. However, concrete+Cr has a smaller I/Io ratio than that of the control concrete. This shows that chromium helps concrete to absorb more photons than a common concrete without additive filler.

The ratio of final to initial intensity between concrete+Mn and the control concrete is also shown in Figure 4 (bottom right). As with the previous samples, concrete+Mn does not show a perfect negative exponential curve. In this case, there is a slight bump at 4 mm thickness. Overall, for any thickness, the I/Io ratio of concrete+Mn is smaller than that of the control concrete. This also suggests that concrete with Mn added absorbs more photons than a common concrete without filler.

The largest gap in the I/Io ratio was observed in the comparison of concrete+steel alloy and the control concrete, as shown in Figure 4 (top left). Here, the concrete+steel alloy is shown as having the smallest I/Io ratio out of all the samples, although all of them showed decreasing I/Io

ratio values, thus indicating improved shielding property in comparison to the control concrete. Based on these curves, the concrete+steel alloy displayed the best performance in terms of ability to absorb and resist photons from x-ray radiation.

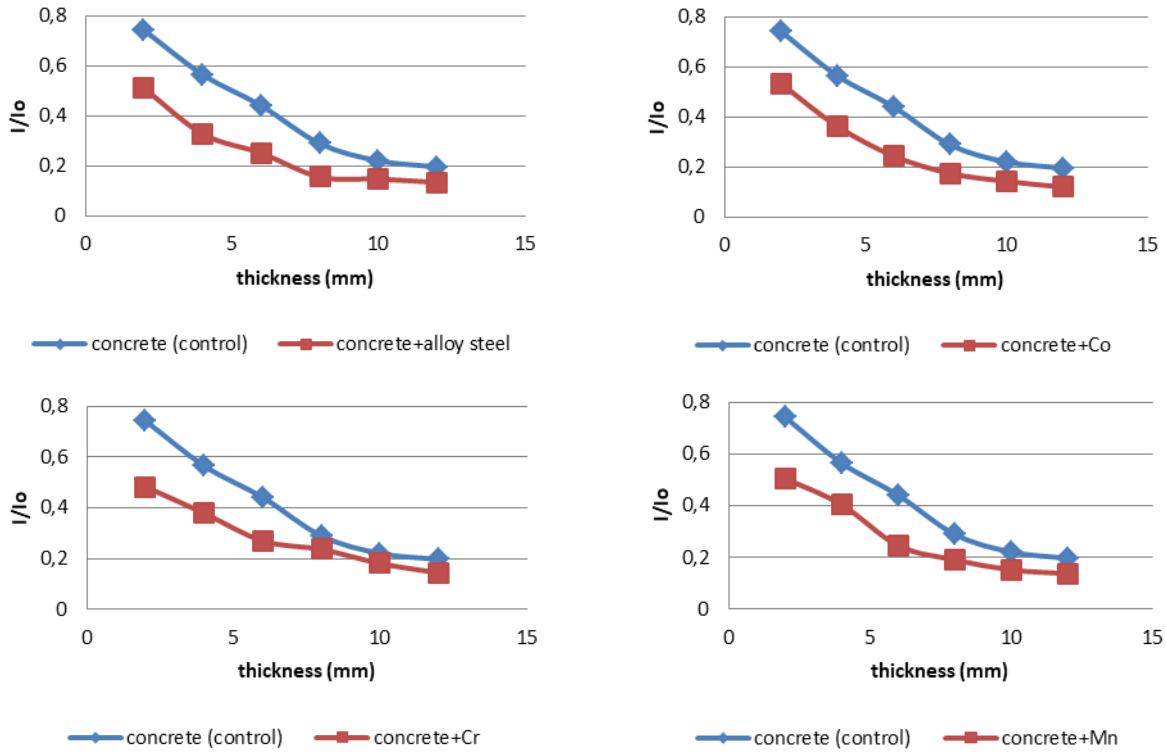

Figure 4 Comparison between the intensity ratios for concrete composite with different fillers added and the control concrete

In general, Figure 4 shows that all of the filled concretes showed an exponentially decreasing trend in intensity ratio, similar to that seen for the control concrete. The curves showed some slight bumps at the different thicknesses of shielding, which are thought to have been caused by imperfections during the synthesization of the control and filled concrete shieldings. This is substantiated by the SEM image of the shielding shown in Figure 5, where we used control concrete filled with Mn to illustrate the apparent inhomogeneity in the mixture.

3.2. Attenuation Coefficient

The attenuation coefficient (μ) of a material indicates the ease with which it can be penetrated by a beam of photons. A large attenuation coefficient indicates that the beam is quickly attenuated or weakened as it passes through the medium. A small attenuation coefficient means that the medium is relatively transparent to the beam. The linear attenuation coefficient describes the fraction of a beam of x-rays or gamma rays that is absorbed or scattered per unit thickness of the material. This value basically accounts for the number of atoms in a cubic cm volume of material and the probability of a photon being scattered or absorbed from the nucleus or an electron of one of these atoms (NDT Resource Center, 2001).

The attenuation is the combination of absorption and scattering in a material. The attenuation of photon intensity is due primarily to a combination of the photoelectric effect, the Compton scattering effect, and pair production. In each case, photon energy is absorbed and transferred to kinetic energy of an electron or an electron-positron pair.

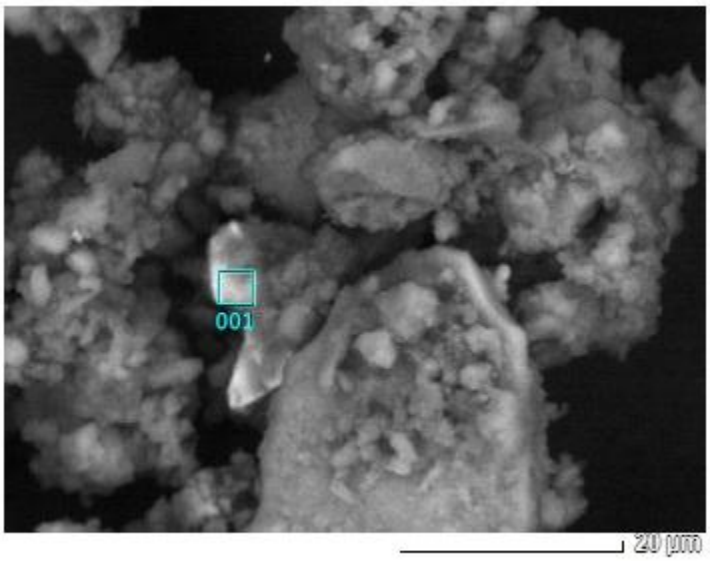

Title	: IMG1
Instrument	: 6510(LA)
Volt	: 20.00 kV
Mag.	: x 2,000
Date	: 2017/04/11
Pixel	: 512 x 384

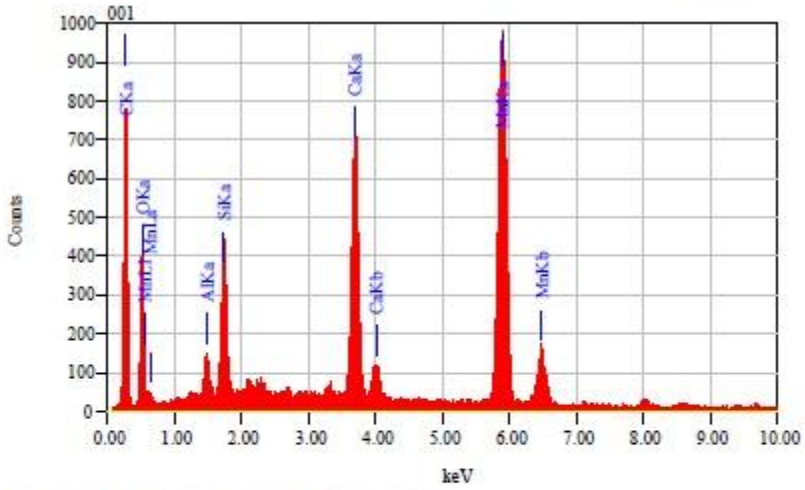

Acquisition Parameter
Instrument : 6510(LA)
Acc. Voltage : 20.0 kV
Probe Current: 1.00000 nA
PHA mode : T4
Real Time : 37.45 sec
Live Time : 30.00 sec
Dead Time : 19 %
Counting Rate: 2146 cps
Energy Range : 0 - 20 keV

ZAF Method Standardless Quantitative Analysis
Fitting Coefficient : 0.2001

Element	(keV)	Mass%	Error%	Atom%	Compound	Mass%	Cation	K
C K	0.277	33.16	0.03	55.23				15.8069
O K	0.525	19.86	0.12	24.84				15.8058
Al K	1.486	1.11	0.05	0.82				1.0117
Si K	1.739	3.41	0.04	2.43				3.8773
Ca K	3.690	9.00	0.05	4.49				16.1124
Mn K	5.894	33.47	0.12	12.19				47.3859
Total		100.00		100.00				

Figure 5 SEM image of Mn-filled concrete shielding (top) and its EDS spectrum (bottom)

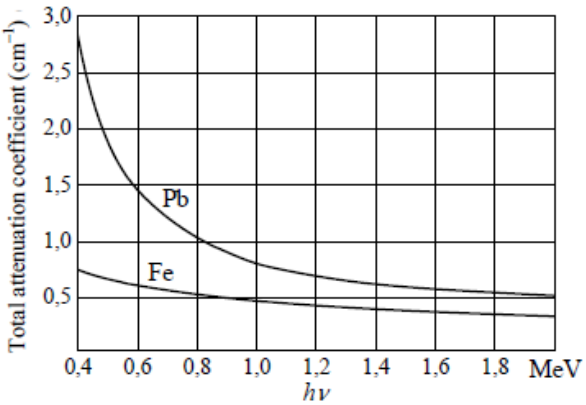

Figure 6 Dependence of the total attenuation coefficient of lead and iron on incident photon energy (Poškus, 2012)

Figure 6 shows the curve of total attenuation due to the sum of these separate components on materials versus the photon energy. It can be seen that attenuation is higher when the photon energy is lower.

Table 1 Linear attenuation coefficient values of the samples measured in the experiments

Thickness (cm)	Linear attenuation coefficient, μ_l (cm^{-1})				
	concrete	concrete + alloy steel	concrete + Co	concrete + Cr	concrete + Mn
0.2	1.4923	3.3620	3.1407	3.6425	3.4126
0.4	1.4286	2.7814	2.5283	2.4266	2.2645
0.6	1.3654	2.2979	2.3450	2.1832	2.3360
0.8	1.5494	2.3174	2.1720	1.8020	2.0694
1.0	1.5088	1.9055	1.9387	1.7065	1.8804
1.2	1.3535	1.6665	1.7565	1.6137	1.6519
Average	1.4497	2.3884	2.3136	2.2291	2.2691

The linear attenuation coefficient was calculated by means of Equation 2 using data obtained from the experiments. The results shown in Table 1 depict considerable variation in the linear attenuation coefficient distribution for each sample. This may be caused by the density variation and inhomogeneous distribution of filler during preparation of the samples. The table shows that the highest average linear attenuation coefficient was found in concrete+steel alloy, i.e, 2.388 cm^{-1}, then in concrete+Co, at 2.314 cm^{-1}, in concrete+Mn, with 2.269 cm^{-1}, concrete+Cr, with 2.229 cm^{-1}, and, finally, in the common concrete without filler (control concrete), at 1.450 cm^{-1}. These values are higher than those reported by (Mirmazhari et al., 2017) because less photon energy was used in this experiment.

The results show that they correspond to atomic number sequence, whereby the atomic number of Co = 27 > Mn = 25 > Cr = 24. The alloy steel composition also consists of elements with higher atomic numbers, including Fe = 26, Ni = 28, Cr = 24, Mn = 25, and Nb = 41. The control concrete has the smallest attenuation coefficient as it contains no filler element. A higher atomic number indicates a higher number of electrons in the atom, meaning there would be more interactions between the photons as x-rays/gamma rays and the electrons of the material. The higher the level of interaction that occurs, the more the photons are depleted of energy, thus producing a better shielding performance.

The experimental linear attenuation values were compared to the results obtained from simulation using the MCNP5 code, as shown in Figure 7. In the Monte Carlo calculation, we used two photon energies (0.041 and 0.042 MeV) of the radiation source to simulate the actual experiments. Figure 7 depicts that as the energy of the incident photon is increased, Monte Carlo simulation shows that the linear attenuation coefficients will decrease. The linear attenuation coefficients according to the simulation were calculated in the same way as for the experiments explained above, i.e., using Equation 2, where the intensity ratio (I/Io) was obtained from the results of the MCNP5 run.

A comparison between the experimental measurements and computer simulation results for each of the samples reveals similar tendencies for the changes to the attenuation coefficients. The discrepancy between the experimental and simulation results is thought to be due to deficiencies in the stirring and mixing of the filler elements added to the concrete composites, which may have resulted in inhomogeneity of the mixtures. Taking everything into account, however, the introduction of 6.06 w% of these filler elements into Portland-type cement-based concrete composites improved the attenuation coefficient of the composites by 40 to 60%. It has

also been shown that out of all the filler elements, concrete with alloy steel filler exhibited the largest improvement in linear attenuation coefficient value.

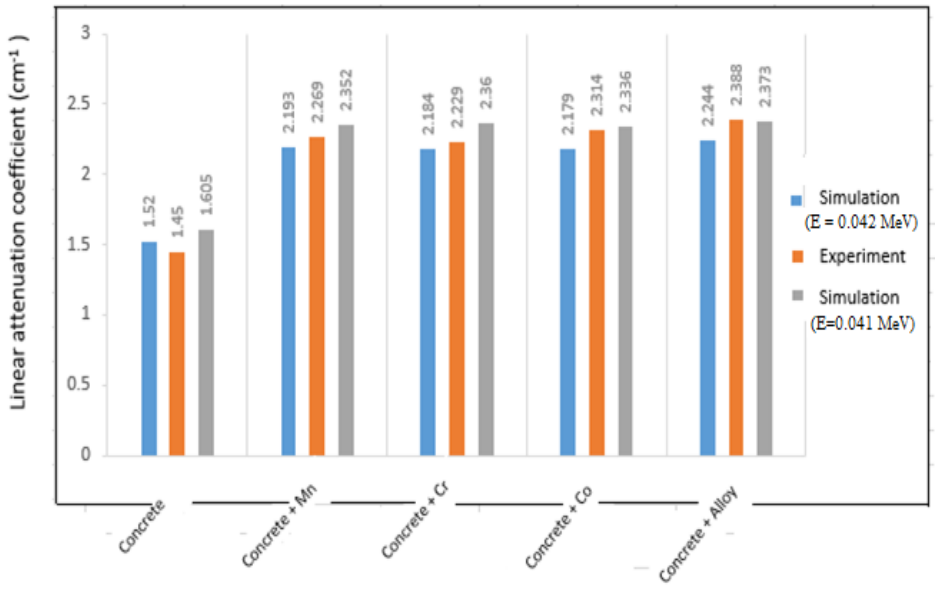

Figure 7 Comparison of linear attenuation coefficients (experiment vs. simulation)

4. CONCLUSION

This study has shown that the synthesization of Portland-type cement-based concrete composite with added filler elements improves x-ray/gamma ray shielding performance, as indicated by the larger linear attenuation coefficients. The shielding capability of the materials as shown by Monte Carlo simulation was inversely proportional to the photon energy applied. The greater the amount of photon energy used, the larger the I/Io ratio became and the smaller the attenuation coefficient that was obtained. It was also demonstrated that each of the concrete composite samples, with 6.06 w% of alloy steel, Co, Cr, and Mn fillers added, respectively, enhanced the x-ray/gamma ray shielding capability of ordinary concrete composites by improving their attenuation coefficient values by 40–60%. In particular, the concrete composite with alloy steel added showed the best shielding performance.

5. ACKNOWLEDGEMENT

The authors wish to thank Dr. Tony Ibnu Suaryada of the Physics Department, Faculty of Mathematical and Natural Sciences, Bogor Agricultural University, Indonesia, for his valuable advice and discussion. We also thank the Center for Empowerment of Informatics and Nuclear Strategic Area of The National Nuclear Energy Agency of Indonesia for providing technical assistance. This work was funded by DIPA BATAN.

6. REFERENCES

Aghamiri, S.M.R., Mortazavi, S.M.J., Shirazi, M.A.M., Rahmani, F., Amiri, A., Jarideh, S., 2014. Production of a Novel High Strength Heavy Concrete using Tourmaline and Galena for Neutron and Photon Radiation Shielding. *International Journal of Radiation Research*, Volume 12(3), pp. 277–282

Akkurt, I., Akyildirim, H., Mavi, B., Kilincarslan, S., Basyigit, C., 2010. Radiation Shielding of Concrete Containing Zeolite. *Radiation Measurements*, Volume 45(7), pp. 827–830

Al-Hamarneh, I. F., 2017. Investigation of Gamma-ray Shielding Effectiveness of Natural Marble Used for External Wall Cladding of Buildings in Riyadh, Saudi Arabia. *Results in Physics*, Volume 7, pp. 1792–1798

Aminian, M., Bakhshandeh, M., Allahbakhshian-Farsani, M., Bakhshandeh, E., Shakeri, N., 2017. Comparison of the Protection Performance in a Composite Shield and a Lead Standard Shield in Terms of Biological Effects in Nuclear Medicine. *Iranian Journal of Nuclear Medicine*, Volume 25(2), pp. 129–135

Arpansa, 2014. What is the Electromagnetic Spectrum? Available online at https://www.arpansa.gov.au/understanding-radiation/what-is-radiation, Accessed on March 23, 2018

Azeez, A.B., Mohammed, K.S., Abdullah, M.M.A.B., Hussin, K., Sandu, A.V., Razak, A.R., 2013. The Effect of Various Waste Materials' Contents on the Attenuation Level of Anti-radiation Shielding Concrete. *Materials*, Volume 6(10), pp. 4836–4846

Elbashir, B.O., Dong, M.G., Sayyed, M.I., Issa, S.A.M., Matori, K.A., Zaid, M.H.M., 2018. Comparison of Monte Carlo Simulation of Gamma Ray Attenuation Coefficients of Amino Acids with XCOM Program and Experimental Data. *Results in Physics*, Volume 9, pp. 6–11

El-Kameesy, S.U., Kansouh, W.A., Salama, E., El-Mansy, M.K., El-Khateeb, S.A., Megahid, R.M., 2017. A Developed Material as a Nuclear Radiation Shield for Personal Wearing. *Journal of Applied Mathematics and Physics*, Volume 5(3), pp. 596–605

Erol, A., Pocan, I., Yanbay, E., Ersoz, O., Lambrecht, F., 2016. Radiation Shielding of Polymer Composite Materials with Wolfram Carbide and Boron Carbide. *Radiation Protection and Environment*, Volume 39(1), pp. 3–6

Fugaru, V., Bercea, S., Postolache, C., Manea, S., Moanta, A., Petre, I., Gheorghe, M., 2015. Gamma Ray Shielding Properties of Some Concrete Materials. *Acta Physica Polonica A*, Volume 127(4), pp. 1427–1429

IAEA, 2014. Radiation Protection and Safety of Radiation Sources: International Basic Safety Standards (GSR Part 3). International Atomic Energy Agency (IAEA), Vienna

Jubier, N.J., 2017. Estimation of Radiation Shielding Properties for Composites Material Based Unsaturated Polyester Filled with Granite and Iron Particles. *Journal of Multidisciplinary Engineering Science Studies* (JMESS), Volume 3(1), pp. 1309–1316

Kim, D.H., Gil, C., Kim, J., Chang, J., 2003. Comparisons of the MCNP Criticality Benchmark Suite with ENDF/B-VI8, JENDL-33, and JEFF-30 (JAERI-Conf--2003-019-PT1), Japan

Kim, J.H., Seo, J.M., Kim, G.J., 2018. Analysis on the Photoneutron According to the Varying Factors and Treatment Planning in LINAC. *Optik*, Volume 156, pp. 424–432

Kim, S.C., Jung, H.M., 2013. A Study on Performance of Low-dose Medical Radiation Shielding Fiber (RSF) in CT Scans. *International Journal of Technology*, Volume 4(2), pp. 178–187

Knoll, G.F., 2000. Radiation Detection and Measurement (3rd ed.). New York: John Wiley & Sons, Inc

Kozlovska, M., Cerny, R., Otahal, P., 2015. Attenuation of X and Gamma Rays in Personal Radiation Shielding Protective Clothing. *Health Physics*, Volume 109(3), pp. 205–211

Kumar, V., Mann, K.S., Manohara, S.R., Sidhu, G.S., 2012. Investigations on Some Low – Z Alkali Minerals as Gamma-Ray Shields. *International Journal of Latest Research in Science and Technology*, Volume 1(4), pp. 324–333

Lumen Learning, 2018. Distinction between X-Rays and Gamma Rays. Available online at https://courses.lumenlearning.com/boundless-physics/chapter/the-electromagnetic-spectrum/, Accessed on March 28, 2018

Mirmazhari, S.S., Entezari, A., Emami Azadi, M.R., 2017. Determination of Mechanical Characteristics and Radiation Attenuation Coefficients of Heavyweight and Normal-

Weight Concretes Containing Hematite for 70 KeV and 570 KeV ϒ-Rays. *International Journal of Civil Engineering, Construction and Estate Management*, Volume 5(2), pp. 13–23

NDT Resource Center, 2001. Transmitted Intensity and Linear Attenuation Coefficient. Available online at https://www.nde-ed.org/EducationResources/CommunityCollege/Radiography/Physics/attenuationCoef.htm, Accessed on February 25, 2018

Nikjoo, H., Uehara, S., Emfietzoglou, D., 2012. *Interaction of Radiation with Matter*. Boca Raton, FL: CRC Press

Oto, B., Gür, A., 2013. Gamma-ray Shielding of Concretes including Magnetite in Different Rate. *International Journal of Physical Sciences*, Volume 8(8), pp. 310–314

Poškus, A., 2012. *Experiment No. 10. Attenuation of Gamma Rays*. Laboratory of Atomic and Nuclear Physics, Vilnius University

Smolikov, A., Pavlenko, V., Shapovalov, N., Kuprieva, O., Solokha, A. 2013. Super Heavy Nano-reinforcing Concrete for Quick Neutron Reactors. *International Journal of Research in Mechanical Engineering & Technology*, Volume 3(2), pp. 28–30

X-5 Monte Carlo Team, 2003. *MCNP - Version 5*, Vol. 1: Overview and Theory. LA-UR-03-1987